Dynamics of guest molecules in PHTP inclusion compounds as probed by solid-state NMR and fluorescence spectroscopy

G. Srinivasan,[a] J. A. Villanueva-Garibay,[a] K. Müller,*[ab] D. Oelkrug,[c] B. Milian Medina,[de] D. Beljonne,[d] J. Cornil,[d] M. Wykes,[d] L. Viani,[d] J. Gierschner,*[cdf] R. Martinez-Alvarez,[g] M. Jazdzyk,[g] M. Hanack[g] and H.-J. Egelhaaf†*[ch]

Received 18th November 2008, Accepted 12th March 2009
First published as an Advance Article on the web 1st April 2009
DOI: 10.1039/b820604j

Partially deuterated 1,4-distyrylbenzene (**2PV**) is included into the pseudohexagonal nanochannels of perhydrotriphenylene (PHTP). The overall and intramolecular mobility of **2PV** is investigated over a wide temperature range by ^{13}C, ^{2}H NMR as well as fluorescence spectroscopy. Simulations of the ^{2}H NMR spectral shapes reveal an overall wobble motion of **2PV** in the channels with an amplitude of about 4° at $T = 220$ K and 10° at $T = 410$ K. Above $T = 320$ K the wobble motion is superimposed by localized 180° flips of the terminal phenyl rings with a frequency of 10^6 Hz at $T = 340$ K. The activation energies of both types of motions are around 40 kJ mol^{-1} which imply a strong sterical hindrance by the surrounding PHTP channels. The experimental vibrational structure of the fluorescence excitation spectra of **2PV** is analyzed in terms of small amplitude ring torsional motions, which provide information about the spatial constraints on **2PV** by the surrounding PHTP host matrix. Combining the results from NMR and fluorescence spectroscopy as well as of time-dependent density functional calculations yields the complete potential surfaces of the phenyl ring torsions. These results, which suggest that intramolecular mobility of **2PV** is only reduced but not completely suppressed by the matrix, are corroborated by MD simulations. Unrealistically high potential barriers for phenyl ring flips are obtained from MD simulations using rigid PHTP matrices which demonstrate the importance of large amplitude motions of the PHTP host lattice for the mobility of the guest molecules.

1. Introduction

Polyconjugated chromophores such as poly(phenylenevinylene)s and polythiophenes are widely used in organic optoelectronic devices. However, applications are limited by the reduction of luminescence efficiency due to aggregation effects[1,2] and by low photostability.[3–5] The inclusion of oligomeric chromophores into channel-forming host materials such as perhydrotriphenylene (PHTP, see Fig. 1) provides a solution to these problems.[6–16] In the presence of rod-shaped oligomers, such as 1,4-bis[(*E*)-2-phenylvinyl]benzene (**2PV**, see Fig. 1), PHTP forms a pseudo-hexagonal host-lattice with parallel **2PV** filled channels.[7,8,17] In the crystal structure of pure PHTP, no channels are formed. This implies that in the host–guest compound the guest must be in close contact to the host. Thus, it is expected that the mobility of **2PV** in the channels is significantly restricted as compared to solution or gas phase. The mobility of the included π-oligomer is of significance in high-precision calculations of excitation energy transfer in light harvesting devices,[18,19] and in the design of functional architectures which require a certain extent of molecular mobility, such as molecular switches. The possible degrees of freedom of guest molecules in the PHTP matrix comprise both intramolecular and overall motions. Intramolecular motions of **2PV** are mainly the torsional vibrations and hindered rotations of the phenyl rings around the formal single bonds. The torsional vibrations of **2PV** depend sensitively on the rigidity of the environment as has been shown by fluorescence studies in liquid and solid solutions.[20] Thus, **2PV** represents the ideal molecule for probing the effect of the matrix on the intramolecular mobility of guest molecules in inclusion compounds.

However, fluorescence spectroscopy is restricted to monitoring those molecular motions which are coupled to electronic transitions. In contrast, NMR spectroscopy offers the opportunity to obtain full 3D characterizations of

[a] *Institute for Physical Chemistry, University of Stuttgart, Pfaffenwaldring 55, 70569, Stuttgart, Germany*
[b] *Dipartimento di Ingegneria dei Materiali e Tecnologie Industriali, Universitá degli Studi di Trento, via Mesiano 77, I-38100, Italy and INSTM, Trento, UdR Trento, Italy. E-mail: k.mueller@ipc.uni-stuttgart.de, klaus.mueller@ing.unitn.it*
[c] *Institute for Physical Chemistry, University of Tübingen, Auf der Morgenstelle 8, 72076, Tübingen, Germany*
[d] *Laboratory for Chemistry of Novel Materials, University of Mons-Hainaut, Place du Parc 20, 7000, Mons, Belgium*
[e] *Institute for Molecular Science, University of Valencia, P.O. Box 22085, 46071, Valencia, Spain*
[f] *IMDEA Nanoscience, Madrid, Spain. E-mail: johannes.gierschner@imdea.org*
[g] *Institute for Organic Chemistry, University of Tübingen, Auf der Morgenstelle 18, 72076, Tübingen, Germany*
[h] *Christian-Doppler Laboratory for Surface-Optical Methods, Johannes-Kepler-University, Altenbergerstr. 69, 4040, Linz, Austria. E-mail: hegelhaaf@konarka.com*
† Present address: Konarka Technologies GmbH, Landgrabenstr. 94, D-90443 Nürnberg

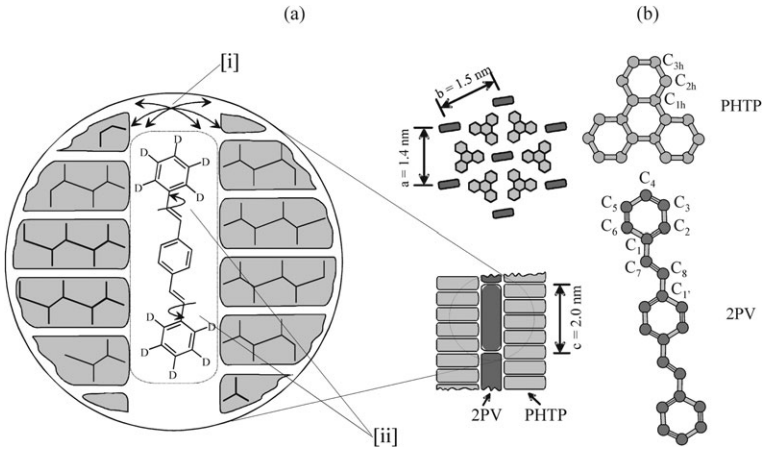

Fig. 1 (a) Schematic structure of the **2PV-d_{10}**/PHTP inclusion compound. Left and lower right: view perpendicular to the crystal *c*-axis; upper right: view parallel to the *c* crystal axis (i—wobble motion of **2PV**; ii—torsional vibrations around the formal single bonds of **2PV**); (b) chemical structures of guest and host components.

molecular mobilities in restricted volumes.[21,22] It has been applied to a variety of inclusion compounds of small molecules and polymers in organic and inorganic hosts.[21,23–43] From ^{2}H and ^{13}C NMR studies it has been found for small molecules such as cyclohexane,[36,41] cyclohexane derivatives[33,41] or trioxane[21,41] that intramolecular motions such as ring inversions are basically not affected by the host. Even for overall rotations, as for instance for benzene guests,[35,38] rather small activation energies have been reported. ^{13}C and ^{2}H NMR studies on PHTP inclusion compounds with alkane guests have shown that also hydrocarbon chains possess an appreciable mobility.[26,28,29] In this case, librations at a number of consecutive bonds introduce large amplitude reorientations of the C–^{2}H-bonds by introducing local twisting of the polymer chain. Recent investigations of α,ω-alkyl-oligothiophenes in tris(*o*-phenylenedioxy)spirocyclotriphosphazene (TPP) have shown that the terminal alkane chains act as hinges around which the central bithiophene moiety rotates in a quasi-free way.[34]

Molecular dynamics (MD) simulations and quantum chemical calculations[44–49] provided a detailed insight into the mechanisms of molecular motions and showed that the roles of the organic "zeolites", such as PHTP and TPP, are completely different from that of real zeolites. Whereas zeolites form fairly rigid channels, the shape and size of the PHTP channels are variable to a certain degree. The interior of the channels and the cross-section depend on the shape of the included molecule and in turn determines the guest mobility. Thus, guest molecules which have a cylindrical shape induce cylindrical PHTP channels and show much higher mobility than found for guests which induce distortions of the hexagonal symmetry of the channel.[44,46] The importance of the dynamic nature of the nanochannel walls for the mobility of the guest molecules becomes obvious from the fact that the results from MD simulations are only in accordance with the NMR results if the artificial constraint of rigidity of the PHTP matrix is removed.[44] In summary, NMR experiments and MD simulations of host–guest compounds revealed an amazing degree of mobility for the included molecules. However, it also becomes clear that the actual degree of freedom depends sensitively on the structure of the guest species.

In this contribution we report on the intramolecular and overall mobility of **2PV**, a representative of the class of phenylenevinylene oligomers and polymers, in PHTP. We present variable temperature fluorescence and ^{2}H NMR investigations on the PHTP inclusion compound with two selectively deuterated **2PV**s. Both spectroscopic methods yield independent information about molecular dynamics of the guest species and thus allow us to obtain a detailed picture of the mobility of a medium sized guest molecule in the nanochannels of PHTP. In particular, ^{2}H NMR is able to distinguish between intramolecular motions, such as phenyl ring flips and overall (hindered) reorientations of the molecule around its principal axis. The combination of fluorescence spectroscopy and quantum chemical calculations allows to model the barrier height for torsional motion. The work is completed by MD simulations which should give independent evidence for the experimentally detected motional contributions of the guest species.

2. Experimental

Synthesis and sample preparation

1,4-Bis[(*E*)-2-phenylvinyl]benzene-d_{10} (2PV-d_{10}) was prepared following a two-step synthetic procedure (see Scheme 1). Thus, (chloromethyl)benzene-d_5 (Aldrich) reacts with triphenylphosphine (Fluka) in xylene to form benzyl(triphenyl)-phosphonium-d_5 chloride **1**. The classical Wittig reaction[50] of the phosphonium salt **1** with terephthaldehyde (Fluka) affords the deuterated compound 2PV-d_{10}.

1,4-Bis[(*E*)-2-phenylvinyl]benzene-d_2 (2PV-d_2) was prepared in an analogous procedure (see Scheme 1) from (chloromethyl)-benzene (Aldrich) and terephthaldehyde-d_2 (Aldrich).

Perhydrotriphenylene was kindly provided by Dr. Borchers (BASF, Ludwigshafen, Germany). Binary inclusion compounds were crystallized from solutions of PHTP and **2PV** (weight ratio 2 : 1) in methylethylketone.[51] Ternary inclusion compounds, PHTP/**1PV**/**2PV**, were crystallized from

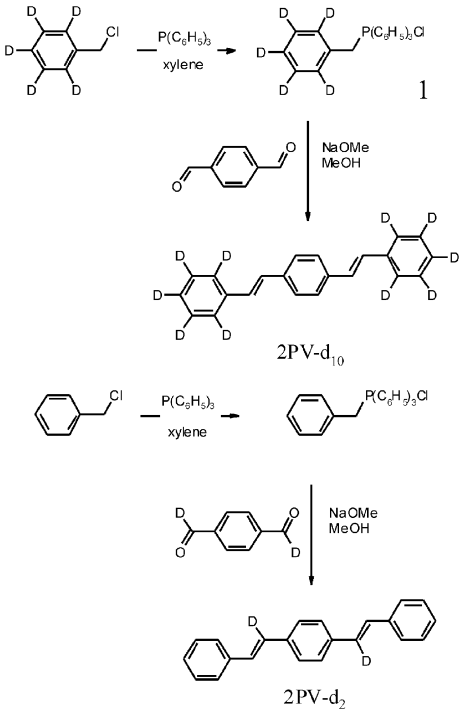

Scheme 1 Preparation of deuterated **2PV-d$_{10}$** (top) and **2PV-d$_2$** (bottom).

solutions of PHTP, stilbene (**1PV**), and **2PV** (weight ratio $2:1:10^{-3}$) in methylethylketone. The obtained crystal needles were isolated, washed with cold methylethylketone and dried in vacuum.

The guest/host molar ratios were determined by fluorometry, UV/VIS absorption, and ^{1}H NMR spectroscopy. The UV/VIS and fluorescence spectra of a given amount of inclusion compound were recorded after dissolution in dioxane. The results were compared with the fluorescence intensity and the absorbance of the pure guest in the same solvent. ^{1}H NMR intensities of methylethylketone were between 0 and 1%; thus solvent co-inclusion in PHTP can be neglected.

Fluorescence experiments

Steady-state fluorescence and fluorescence excitation spectra were recorded on a SPEX 222 fluorometer equipped with Glan-Thompson polarizers (Instruments S A., Longjumeau, France). The light source was a 450 W Xe arc lamp, the detector was a R928 photomultiplier tube. Fluorescence excitation spectra are corrected for excitation intensity with the help of a rhodamine B quantum counter. Emission spectra are corrected for the sensitivity of the detection system with a correction file. 10^{-7} M solutions of **2PV** in EPA (a mixture of diethylether, i-pentane, and ethanol) were prepared using Merck UVASOL solvents. Unpolarized fluorescence spectra of inclusion compounds were obtained on powders of randomly oriented crystallites which were pressed onto fused silica or aluminium substrates. For low-temperature measurements the samples were cooled down by a closed-cycle He cryostat.

^{13}C NMR experiments

^{13}C MAS NMR spectra were recorded at 75.47 MHz on a CXP 300 Bruker (Bruker/Rheinstetten) spectrometer (magnetic field strength: 7.04 T) equipped with a Tecmag control unit and using a standard 4 mm Bruker MAS probe. All magic angle spinning experiments were done at the sample spinning rate of 5 kHz applying either single pulse (SP) or cross polarization (CP) excitation schemes (contact time: 1 ms). The $\pi/2$ pulse widths for carbon and protons were 4 μs. Recycle delays were chosen to 20 and 60 s for CP and SP ^{13}C NMR experiments, respectively. ^{13}C chemical shifts were determined relative to the external standard adamantane. All ^{13}C chemical shifts are expressed relative to tetramethylsilane (TMS) with $\delta = 0$ ppm.

^{2}H NMR experiments

All ^{2}H NMR measurements were carried out on a Bruker CXP 300 spectrometer (Bruker/Rheinstetten) operating at a frequency of 46.07 MHz for deuterium, by using a standard (liquid nitrogen flow) 5 mm double-resonance probe ($\pi/2$ pulse length = 2 μs). The variable temperature ^{2}H NMR spectra were recorded by applying the quadrupole echo sequence $[(\pi/2)_x$–τ_e–$(\pi/2)_y$–τ_e-acquisition] with pulse intervals τ_e as given in the text. The number of scans varied between 1024 and 2560 for **2PV-d$_{10}$** or between 8000 and 10 000 for **2PV-d$_2$** depending on the S/N ratio, and the recycle delay between successive scans was 20 s. The sample temperature was controlled by a Bruker BVT 1000 unit. The accuracy of the temperature was within ±1 K.

NMR data processing

The data processing of the experimental and simulated NMR signals was performed on a SUN Sparc 10 workstation using the NMRi and Sybyl software packages (Tripos, St. Louis).

^{2}H NMR simulations

NMR line shape simulations were done with appropriate FORTRAN programs, developed in our group for the behaviour of an isolated I = 1 spin system for different types of dynamic NMR experiments.[21,38,43] The simulation programs are very general and take into account various types of molecular motions of the system under investigation. In all simulations, the final best fit was chosen by direct comparison between experimental and theoretical spectra, taking into account the overall appearance of the line shapes as well as their relative amplitudes.

Quantum chemical calculations

Quantum-chemical calculations of the vibrational frequencies in the electronic ground and the first excited state were performed at the (time-dependent) density functional theory level of theory, (TD)-DFT, using Becke's three-parameter B3LYP exchange–correlation functional[52] with the 6-311G* basis set[53] within the TURBOMOLE V5-7 package.[54] Torsional potentials for the outer phenyl rings in the ground and first excited state were obtained from systematic variation of the torsional angle around the C_1–C_7 bond, keeping C_2 symmetry, and subsequent calculation of the single point ground and excited-state energies. The absorption spectrum was calculated using an in-house programme by mirroring the emission spectrum at the electronic origin and convoluting the

spectrum with the line spectrum, $G(\tilde{\nu})$, of the torsional modes as obtained for transitions between the vibrational quanta v in the S_0 state and the vibrational quanta w in the S_1 state within the model of distorted, undisplaced oscillators.[20]

Molecular dynamics simulations

The intramolecular mobility of **2PV** *in vacuo* and in a periodic PHTP system was investigated by molecular dynamics (MD) simulations using the molecular modeling package TINKER 4.2,[55] and by molecular mechanics (MM) using the force field MM3. To obtain an accurate description of the potential for the rotation of the phenyl rings around the outer single bonds, the MM3 torsional parameters were modified in order to reproduce the DFT potential described above. The periodic PHTP cell with empty channels was built from the X-ray structure of a similar compound[6] and the guest was subsequently inserted in the channels. One repetition cell contained four **2PV** molecules and 40 PHTP molecules, yielding a dye concentration of $C_{\mathbf{2PV}} = 0.33$ M, somewhat smaller than the value found experimentally ($C_{\mathbf{2PV}} = 0.48$ M). However, it is not expected that this affects the torsional barrier. MD simulations of the periodic structure were then performed in the NPT ensemble using the Andersen thermostat to maintain a temperature of 300 K and the Berendsen barostat to maintain a pressure of 1 atmosphere. Non-bonded forces were calculated with atom-based cutoffs of 10.0 Å. MD simulations *in vacuo* used the same thermostat and cutoff. Torsional potentials were mapped out by recording the change of the angle $C_2C_1C_7C_8$ (see Fig. 1) during the MD run, thus giving a probability histogram. The corresponding potential was then obtained *via* the Boltzmann equation. A drawback of this method is the poor sampling in the regions where the potential barrier reaches its maximum. Thus, the error in the calculated potential barrier in these regions is large. To avoid this source of error and to improve the quality of the results, an umbrella potential was applied to increase sampling of energetically unfavorable angles. The weighted histogram analysis method (WHAM)[56] was then applied to the resulting distributions to remove the effect of the umbrella potential and provide a well defined torsional free energy profile over the full range of the torsion.

3. Results and discussion

3.1 NMR spectroscopy

3.1.1 ^{13}C NMR studies. Representative ^{13}C MAS NMR spectra of the **2PV**/PHTP, **2PV-d$_2$**/PHTP inclusion compounds and pure **2PV-d$_2$** are given in Fig. 2. The assignment of the signals and the corresponding ^{13}C chemical shift values are indicated in the Figure and are summarized in Table 1. It can be seen that the ^{13}C resonances of the **2PV** guests in PHTP are almost identical to those reported for pure **2PV** or poly(*p*-phenylene vinylene), indicating negligible influence by the incorporation into the PHTP matrix.[57–59] Likewise, the ^{13}C shifts of PHTP are in agreement with former published values.[27,60] The experimental ^{13}C NMR spectra at 220 K are somewhat better resolved than those at $T = 300$ K, which can be traced back to the presence of guest motions interfering with the rf decoupler field at elevated temperatures.[61,62]

The presence of guest motions is also evident from the enhanced signal intensity of the **2PV** signals in the single pulse (SP) experiments (Fig. 2e and f) as compared to the corresponding ^{13}C CP/MAS experiment (Fig. 2c and d). That is, polarization transfer during contact time is slower for mobile species, here **2PV**, as compared to that of the rigid structural components, *i.e.* the PHTP host molecules, resulting in reduced signal intensities of the former ones during the CP experiment. In principle, it should be possible to extract further information about the dynamic properties of the guest species from such ^{13}C NMR experiments, for instance by analyzing the spinning side bands or *via* relaxation studies, supposed the size and orientation of the ^{13}C chemical shift tensors and of the ^{13}C–^{1}H dipolar couplings are known. The former information is only accessible through the analysis of single crystal experiments which were not available in the present case.

3.1.2 ^{2}H NMR studies. ^{2}H NMR experiments on selectively deuterated compounds are easier to handle, as the spectra and relaxation are only determined by the well-defined nuclear quadrupolar interaction. In the following, ^{2}H NMR spectroscopy is used to examine the overall and internal (intramolecular) mobility of **2PV** in PHTP inclusion compounds. Hence, **2PV** was deuterated at the outer phenylene rings (**2PV-d$_{10}$**) and at the CH groups next to the inner phenylene ring (**2PV-d$_2$**), as depicted in Fig. 1. Variable temperature ^{2}H NMR experiments were then performed on the respective PHTP inclusion compounds, **2PV-d$_{10}$**/PHTP and **2PV-d$_2$**/PHTP.

In Fig. 3, representative ^{2}H NMR spectra are shown for **2PV-d$_{10}$**/PHTP which were obtained with the quadrupole echo experiment at pulse spacings of $\tau_e = 30$, 60 and 100 μs. All three series of ^{2}H NMR spectra exhibit characteristic line shape changes depending on the actual sample temperature and the pulse spacing τ_e. These findings can be traced back to the presence of distinct guest motion on a timescale which matches the sensitive range of the quadrupole echo experiment, with correlation times τ_e in the order of 10^{-4} to 10^{-8} s. Below 220 K the ^{2}H NMR experiments yield typical "rigid limit" NMR line shapes, where the motional processes are slow and outside the sensitive range.

Heating above 220 K is accompanied by some spectral narrowing along with the appearance of non-axially symmetric ^{2}H NMR line shapes. At around 300 K the ^{2}H NMR spectra with $\tau_e = 30$ μs (left column) are further distorted, as reflected by a loss in signal intensity for the central part of the powder pattern as well as for the inner part of the shoulders. This signal loss becomes even more pronounced at longer pulse delays, $\tau_e = 60$ and 100 μs (central and right columns). It is well known that such spectral alterations are very sensitive to the type and timescale of the underlying molecular processes. Basically, they reflect a distinct anisotropy of the spin–spin relaxation time T_2, arising from motional effects modulating the underlying dominant quadrupolar interaction. Above 340 K additional spectral changes are registered due to a second motional contribution which enters the sensitive time-scale for the NMR experiment.

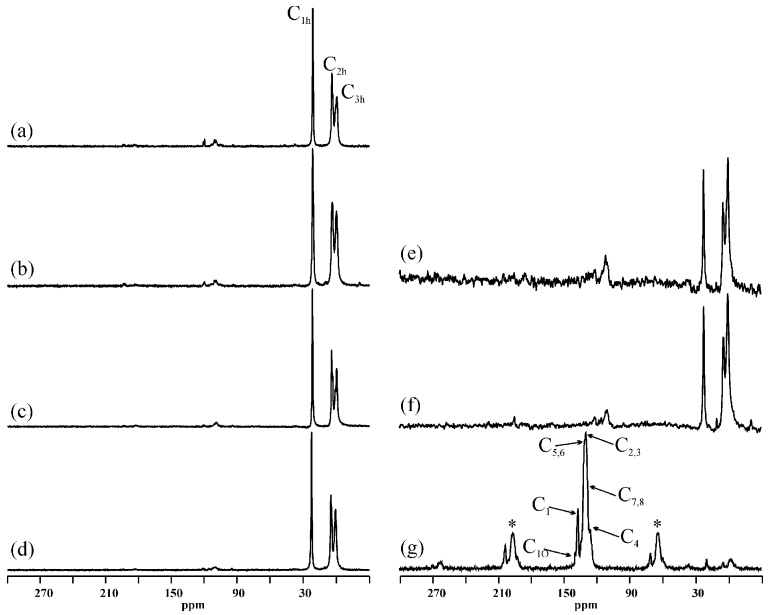

Fig. 2 Experimental ^{13}C MAS NMR spectra at 220 K (a, b) and 300 K (c–g). ^{13}C CP/MAS NMR spectra for **2PV**/PHTP (protonated guests) are given in (a) and (c), while (b) and (d) refer to the corresponding spectra for **2PV-d$_2$**/PHTP. ^{13}C SP/MAS NMR spectra at 300 K for **2PV**/PHTP and **2PV-d$_2$**/PHTP are shown in (e) and (f), respectively. The ^{13}C CP MAS NMR spectrum of pure **2PV-d$_2$** at 300 K is given in (g). Asterisks indicate spinning side bands. The ^{13}C NMR assignments are given in Table 1.

Table 1 ^{13}C chemical shift values in ppm of 2PV-d$_2$, PHTP and related compounds

Guest	δ ($C_{1'}$)	δ (C_1)	δ ($C_{2,3}$)	δ (C_4)	δ ($C_{5,6}$)	δ ($C_{7,8}$)
2PV-d$_2$[a]	138.3	135.7	128.6[b]	125.0	130.1	128.6[b]
DSB[57]	137.1	136.2	128.9	124.4	130.7	127.8
PPV[57]	136.6	—	124.9	—	132.0	128.3
PPV[59]	136.0	—	124.0	—	131.0	128.0
Host	δ (C_{1h})		δ (C_{2h})		δ (C_{3h})	
PHTP[a]	47.8		32.2		28.4	
PHTP[32]	48.4		32.7		28.8	

[a] This work. [b] Not resolved.

In order to reproduce the experimental ^{2}H NMR line shapes of **2PV-d$_{10}$**/PHTP, a series of model calculations was performed, taking into account the particular structural composition of the present sample as well as the data and results from previous work on related systems. It turned out that the present experimental ^{2}H NMR data can be at best reproduced by considering a dominant quadrupolar interaction with typical interaction parameters for aromatic deuterons (coupling constant e^2qQ/h = 185 kHz, asymmetry parameter η = 0.05) and by assuming two superimposed motional processes (see Fig. 1), namely: (i) overall reorientational (wobbling) of the whole guest molecule; and (ii) local 180°-ring flips of the deuterated phenyl rings).

To describe the wobble process we have taken a motional model which was proposed earlier by Vold *et al.*[63] during a study of the biphenyl/α-cyclodextrin inclusion compound. Following this approach, the overall molecular wobbling is described by small angle jumps. Hence, 19 jump sites were chosen in such a way that a network is constructed with one unique site at the pole, 6 sites forming a cone with an opening angle θ, and 12 sites of a second cone with an opening angle 2θ. It is further assumed that exchange only takes place between neighbouring sites.

It should be noted that for the final simulations of the experimental **2PV-d$_{10}$**/PHTP data, two types of non-equivalent deuterons had to be taken into account, namely two deuterons along the *para*-axis and the remaining eight deuterons, whose C–^{2}H bond directions are inclined at an angle of 60° with respect to the p-axis. Thus, the simulated spectra represent a superposition of two sub-spectra with an intensity ratio of 4 : 1. The deuterons with the C–^{2}H bond direction parallel to the *para*-axis are not affected by the ring flip motion at all. For the overall wobbling the situation is different, as it affects all deuterons. However, the effect is different for the aforementioned two groups of deuterons, which is again a consequence of the different orientations with respect to the wobble symmetry axis.

Representative results from model simulations using the 19-site motional process are given in Fig. 4. It is seen that the motional correlation times, the pulse spacing τ_e, and the actual opening angle strongly affect the ^{2}H NMR line shapes. Moreover, the theoretical spectra display the same spectral

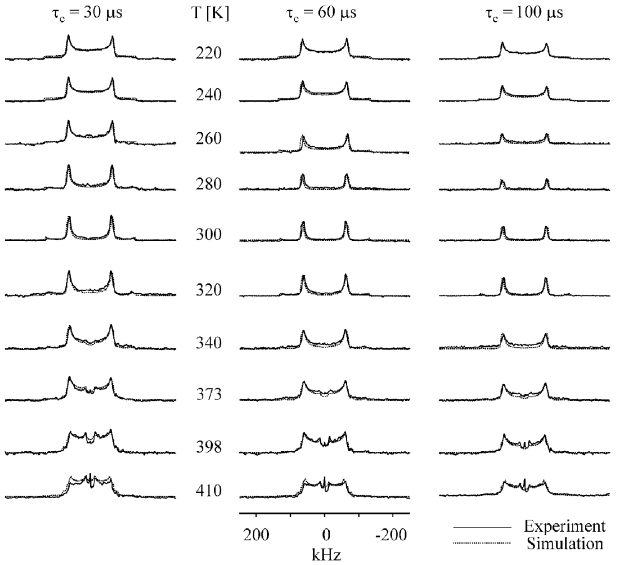

Fig. 3 Experimental and theoretical ^{2}H NMR spectra of **2PV-d$_{10}$** in PHTP obtained from the quadrupole echo experiment with different echo delays τ_e = 30, 60 and 100 μs, respectively. The experimental and simulated spectra are superimposed. Simulation parameters are given in Table 2.

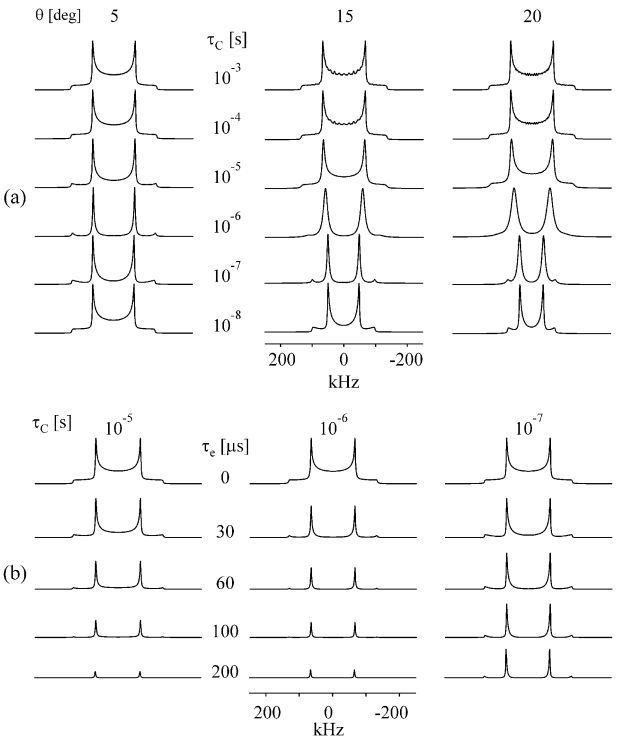

Fig. 4 Theoretical ^{2}H NMR spectra (quadrupolar echo experiment) obtained from the 19-site jump model (overall fluctuations). (a) Influence of correlation times on the general appearance of the line shapes (τ_e = 30 μs) at three different opening angles. (b) Influence of pulse spacing τ_e on the partially relaxed spectra (θ = 5°) at three different correlation times.

features that are registered in the experimental ^{2}H NMR spectra below 340 K. On the basis of these model simulations it was thus possible to reproduce the experimental ^{2}H NMR line shapes of the **2PV-d$_{10}$**/PHTP inclusion compound in the temperature range below 340 K.

For temperatures above 320 K the aforementioned internal 180°-ring flip process had to be superimposed. Representative model simulations demonstrating the influence of this motional contribution on the ^{2}H NMR spectra are given in Fig. 5. Again, both the actual correlation time τ_c and the chosen pulse separation time τ_e have a strong influence on the overall appearance of the corresponding ^{2}H NMR line shapes.

The final results from the best fit simulations of the experimental ^{2}H NMR spectra, based on the combined ring flip/overall wobble model, are given in Fig. 3. In general, a very good reproduction of the experimental spectra could be achieved. It is obvious that a finite jump model for the overall guest motion can only be a crude approach for a diffusive process. It would be therefore natural to increase the number of jump sites, thus approaching the scenario of a diffusive process. However, in view of the present very good agreement between experiment and theory, there was no need to follow up in this direction.

The simulation parameters used for the present ^{2}H line shape calculations are summarized in Table 2. The derived motional correlation times are given in an Arrhenius representation in Fig. 6 which yield activation energies of $E_{A,w} = 43 \pm 2$ kJ mol^{-1} for the overall wobble process, and $E_{A,rf} = 40 \pm 3$ kJ mol^{-1} for the ring flip motion. In addition, the opening angle 2θ was found to vary between 8° at low temperature and 20° at the highest temperature examined here. The pre-exponential factors for the ring-flip and wobble motions were found to $A_{rf} = A = 1.4 \times 10^{12}$ s^{-1}

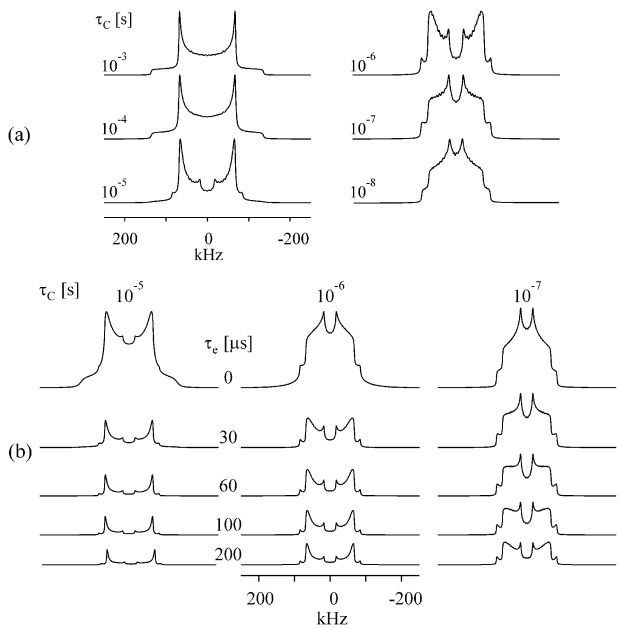

Fig. 5 Theoretical ^{2}H NMR spectra (quadrupolar echo experiment) obtained from the superposition of a 19-site jump model (overall fluctuations, with $\tau_e = 1 \times 10^{-7}$ s, θ = 5°) and 180°-ring flip motions. (a) Influence of 180°-ring flip dynamics on the general appearance of the line shapes (τ_e = 30 μs). (b) Influence of pulse spacing τ_e (19-site jump model) on the partially relaxed spectra at three different correlation times for the 180°-ring flip.

Table 2 Simulation parameters for the ^{2}H NMR line shape analysis of 2PV-d_{10}/PHTP

	Wobble motion		Ring flip
T/K	Correlation time (τ_c)/s	Opening angle θ/deg	Correlation time (τ_c)/s
220	2.5×10^{-4}	4	
240	5.0×10^{-5}	4	
260	1.5×10^{-5}	4	
280	2.0×10^{-6}	4	
300	3.5×10^{-7}	6	
320	1.0×10^{-7}	6	
340	7.0×10^{-8}	7	1.0×10^{-6}
373	3.0×10^{-8}	8	3.0×10^{-7}
398	1.0×10^{-8}	9	1.5×10^{-7}
410		10	8.0×10^{-8}

Quadrupolar coupling constant $e^2qQ/h = 185$ kHz; asymmetry parameter $\eta = 0.05$.

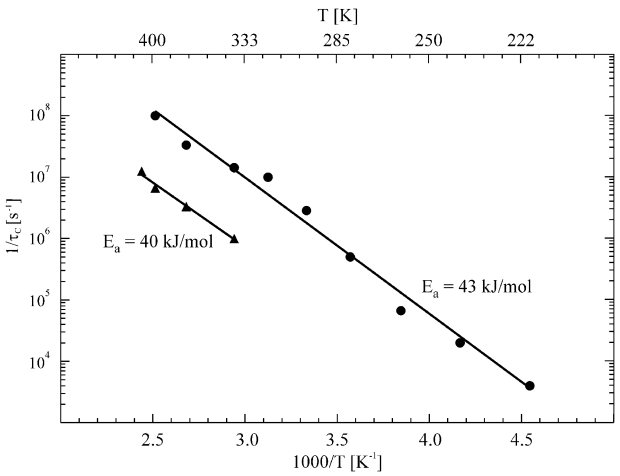

Fig. 6 Arrhenius representation of the correlation times for overall wobble (19-site jump model; circles) and 180°-ring flip motion (triangles) of **2PV-d_{10}** in PHTP.

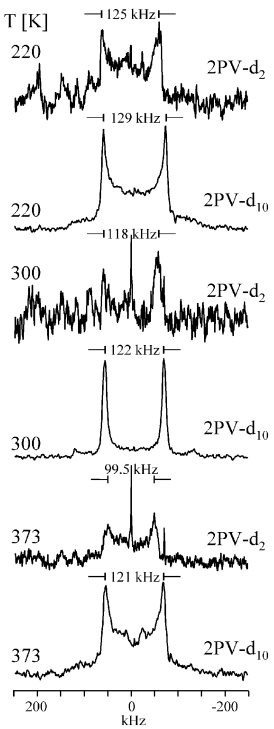

Fig. 7 Experimental ^{2}H NMR spectra for the inclusion compound of PHTP with **2PV-d_2** and **2PV-d_{10}** along with the quadrupolar splitting between the perpendicular singularities.

and $A_w = A = 5.1 \times 10^{13}$ s^{-1}, respectively. It should be noted that we did not go beyond 410 K, since at such elevated temperatures the inclusion compound starts to decompose.

Fig. 7 shows for comparison some representative ^{2}H NMR spectra for **2PV-d_2**/PHTP and **2PV-d_{10}**/PHTP. Both the ^{2}H NMR spectra of **2PV-d_2**/PHTP and **2PV-d_{10}**/PHTP exhibit the same trends, although—due to the low amount of deuterons—the S/N ratio of the former sample is rather poor. Again, for sample **2PV-d_2**/PHTP at 300 K the central part of the NMR line shape breaks down, and a general reduction of the spectral splitting is observed upon increasing temperature. Both observations are again a clear indication for the presence of overall reorientational motions.

However, at 373 K the quadrupolar splitting for **2PV-d_2**/PHTP is found to be smaller than for **2PV-d_{10}**/PHTP, as reflected by the reduction factors of 0.796 and 0.968 (ratios between the quadrupolar splittings at 373 and 220 K). We attribute these discrepancies to additional internal motional contributions (*e.g.* librational motions) in the inner molecular segment which bears the deuteron label. Due to the lack of further information, it is presently not possible to discuss this issue in a quantitative way. In summary, the experimental ^{2}H NMR spectra for **2PV-d_2**/PHTP thus confirm the applied model assumptions during the data analysis of **2PV-d_{10}**/PHTP. A flip motion of the molecule at $T > 320$ K as a whole can be thus excluded.

A comparison of the derived kinetic parameters of the present system with the data from investigations on related PHTP inclusion compounds is difficult. So far only a few solid-state ^{13}C and ^{2}H NMR studies for PHTP inclusion compounds exist, where polymers were used as guest components[28–30,32,33] and which behave quite differently.

In the present case, the local ring-flip motions are found to be slower than the wobble process. The derived correlation times and the activation energy for the ring flip motion fall within the typical range which is discussed for solids with phenyl rings that undergo rotational motion around a C–C single bond (polymers,[22,64,65] proteins, molecular crystals, *etc.*).[66–73] For instance, ^{13}C NMR studies were performed on

poly(*p*-phenylene vinylene) (PPV) films, which have shown that the phenyl rings in both the amorphous and crystalline regions undergo 180°-ring flips with activation energies ranging from 20 to 60 kJ mol^{-1}.[59,73] It is interesting to note that in inclusion compounds also other intramolecular processes, like methyl group rotation, ring inversion or conformational changes, have been examined which again were found to remain almost unaffected by the surrounding host lattice.[21,38,41,43]

3.2 Fluorescence spectroscopy

Earlier polarized fluorescence spectroscopy studies revealed the immobilizing effect of the PHTP matrix on the overall mobility of **2PV**.[8,74,75] In the present work, fluorescence spectroscopy is used to investigate the effect of the PHTP matrix on the *intra*molecular mobility of **2PV**. For this purpose, ternary inclusion compounds of the composition PHTP/**1PV**/**2PV** were prepared, with relative molar concentrations of approximately $9/1/10^{-3}$. **1PV** (= *trans*-stilbene) has one styrene unit less than **2PV** and thus absorbs at shorter wavelengths. **1PV** thus acts as a spectroscopically inactive diluent which is not excited, neither directly by the excitation light nor indirectly by energy transfer, but reduces the concentration of **2PV** to 5×10^{-4} M, so that the absorbances of all samples are well below $A = 0.1$.

The effect of matrix rigidity on the spectra of **2PV** becomes evident upon inspection of Fig. 8a. Fluorescence and fluorescence excitation spectra of **2PV** in PHTP at room temperature (bottom panel) are more structured than in solution (top panel). This effect is most striking for the excitation spectrum, which shows no vibrational structure in solution, but resolved vibronic replica in PHTP. This enhancement of the vibrational structure is a consequence of the reduction of the amplitudes of the torsional motions upon inclusion of **2PV** into PHTP. The shape of the absorption spectra of **2PV** is mainly determined by the amplitudes of the torsional vibrations around the formal single bonds in the electronic ground state (Fig. 9a).[20,76] In liquid solution, several quanta of these torsional vibrations are thermally populated at room temperature. Due to the more quinoid structure of **2PV** in the first excited singlet state, S_1, the potential well for the torsional motion is much steeper in the excited state than in the ground state, S_0.[20] Thus the fluorescence excitation spectrum is blurred by the superposition of transitions originating from different initial states. Upon cooling to $T = 10$ K the vibrational structure of the spectra becomes even better resolved (Fig. 8b). This may be partly due to a steeper potential well for the torsional vibrations by the contraction of the nanochannels. However, fluorescence and fluorescence excitation spectra are affected in the same way. This suggests that the reason for the enhanced resolution is rather the freezing out of low frequency modes, *e.g.* lattice phonons of the host, which leads to reduced inhomogeneous broadening.

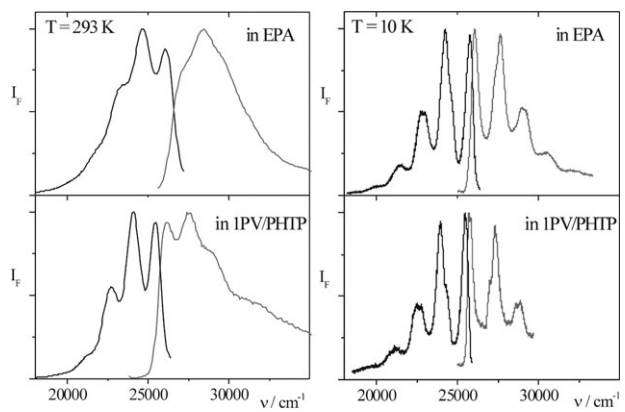

Fig. 8 Fluorescence and fluorescence excitation spectra of **2PV** in EPA (top panel) and in PHTP, coincluded with **1PV** (bottom panel). The molar ratio **2PV**/**1PV** ~ 10^{-3}. Excitation at 27 500 cm^{-1}, observation at 23 500 cm^{-1}. Left panel: at $T = 293$ K, right panel: at $T = 10$ K.

From a comparison of the shapes of the experimental and of the simulated absorption spectra it is possible to estimate the extent to which the torsional mobility is reduced upon inclusion of **2PV** into PHTP. For the simulation of the spectra we follow the method described in the paper by Gierschner *et al.*[20] Oligo(phenylenevinylene)s are assumed to have potential energy minima in their planar conformation of S_0 as well as of S_1. For stilbene (**1PV**), the planar conformation is defined by the torsional angles $\phi = \varphi_1 = \varphi_2 = 0°$ around the two formal single bonds. The adiabatic energy difference between the two electronic states is

$$\Delta E_0 = S_1(\phi = 0) - S_0(\phi = 0) \quad (1)$$

The intramolecular torsional potential energies $P_{n,\mathrm{int}}(\varphi)$ around the terminal carbon–phenyl bond C_1–C_7 in the two electronic states S_n ($n = 0, 1$) are described in first approximation by a parabola,

$$P_{n,\mathrm{int}} = \tfrac{1}{2} k_n \phi^2 \quad (2)$$

with $k_1 > k_0$. This approximation is applicable for small torsional angles. For large angles it is reasonable to introduce rotational potential barriers V_n of finite height

$$P_{n,\mathrm{int}} = V_n \cdot \sin^2\phi, \quad (3)$$

with $V_1 > V_0$. This is the simplest approximation of a two-fold symmetric potential barrier that neglects, *e.g.*, cross terms between the two terminal carbon-phenyl axes. For small torsional angles, eqn (2) and (3) yield very similar results, but not for large angles, since eqn (2) does not allow for 180° phenyl ring flips. In the following, we will first examine **1PV**, where the calculations can be directly compared to experimental gas phase data, before we return to **2PV**.

For **1PV**, where the torsional vibrations are well described by rotations of the phenyl rings around the single bonds, experimental data are available from molecular jet experiments. The derived values are $V_0 = 11$ kJ mol^{-1} = 875 cm^{-1} (3100 cm^{-1}) and $V_1 = 20$ kJ mol^{-1} = 1670 cm^{-1} (3000 cm^{-1}) for the flip of one phenyl ring or both phenyl rings (numbers for the latter case are given in parenthesis).[77] The potentials in the vicinity of the equilibrium conformation have been calculated from the experimental torsional frequencies for the counter-phase torsional motion of the two phenyl

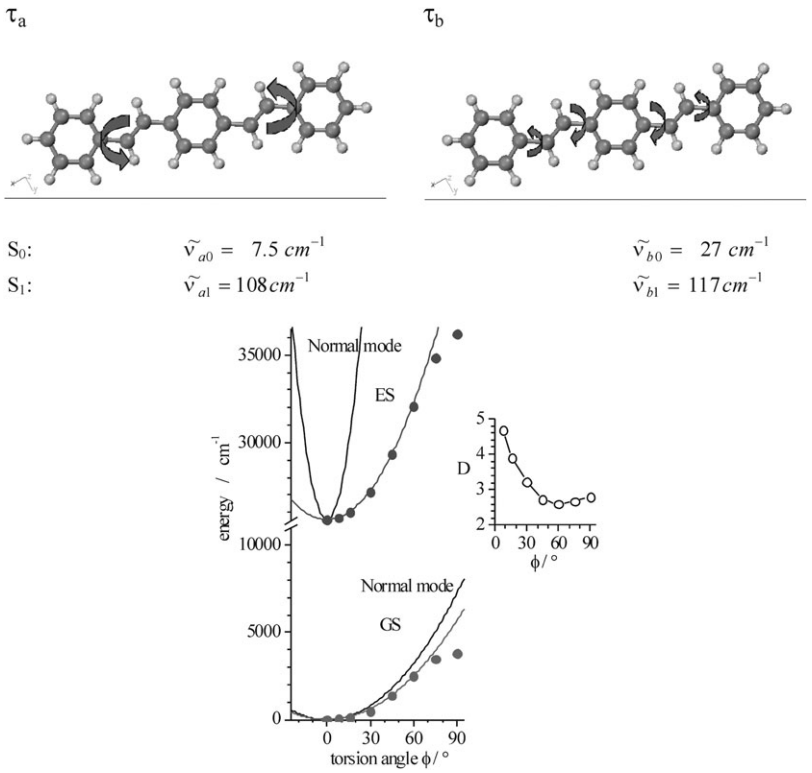

Fig. 9 Top panel: Torsional vibrations τ_a and τ_b of **2PV** with one and two nodes, respectively. The wavenumbers $\tilde{\nu}_{i0}$ and $\tilde{\nu}_{i1}$ are the results of (TD-)DFT B3LYP/6-311G* calculations for the molecule in vacuum and refer to the electronic ground and excited states, S_0 and S_1, respectively. Bottom panel: solid curves are the harmonic potentials for the vibration τ_a in S_0 (GS) and S_1 (ES), calculated from the data in Table 3 using eqn (4). Points are the energies obtained from single point (TD-)DFT calculations for the simultaneous torsion of both terminal phenyl rings around the formal single bonds. Dotted curves through these points are harmonic fits of the points at small torsion angles ($\phi < 30°$). The inset shows the angular dependence of the *D*-factor as calculated from the single point (TD-)DFT potential curves.

rings, $\nu_0 = 9$ cm^{-1} , $\nu_1 = 47$ cm^{-1} and their overtones.[76,77] The ground state potential has been found to be very anharmonic,[76] while the potential in S_1 is well approximated by a harmonic function.[77] We used these experimental data to assess the reliability of our (TD-)DFT (B3LYP/6-311G*) calculations which are presented in Table 3.

Although the frequencies of the vibrations in both, S_0 and S_1, are overestimated by the (TD-)DFT method, the calculations describe the ground state vibration sufficiently well. Assuming approximately harmonic potentials for the torsional vibration in S_0 and S_1, the force constants k'_1 and k'_0 are obtained from the calculated frequencies, ν_{i0}, and the torsional angles in the vibrational ground state, φ_{i0},

$$k'_i = \frac{h\nu_{i0}}{\varphi_{i0}^2} \qquad (4)$$

In the harmonic regime (*i.e.* $\phi < 20°$ for S_0, $\phi < 65°$ for S_1) both harmonic potential curves agree perfectly with the (TD-)DFT single point calculations performed at different torsional angles. Since at room temperature kT corresponds to a torsional angle of about 25°, the harmonic approximation should be a good estimate for the thermal population of the torsional modes. The (TD-)DFT single point calculations of the torsional potentials yielded for the barriers for the simultaneous torsion of two rings in the gas phase $V_0 = 3400$ cm^{-1} and $V_1 = 14\,900$ cm^{-1}. The value for the ground state barrier agrees well with the results of other quantum chemical calculations[78,79] and with the experimental value in the gas phase.[77]

For **2PV**, no experimental data are available for the two low-frequency torsional vibrations, τ_a and τ_b, which couple effectively to the electronic transition $S_0 \rightarrow S_1$. Therefore, the vibrational frequencies and the corresponding potential curves were taken from the results of the density functional ((TD-)DFT) calculations (Table 3). The lowest frequency ($\tilde{\nu}_a = 7.5$ cm^{-1}) torsional vibration, τ_a, in the ground state of **2PV** is described quite satisfactorily by considering only

Table 3 Results of (TD-)DFT calculations for the lowest frequency torsional vibration of **1PV** and **2PV**

	1PV		**2PV**	
	S_0	S_1	S_0	S_1
$\tilde{\nu}$/cm^{-1}	12	111	7.5	108
μ/g mol^{-1}	3.586	3.812	3.953	3.790
k_i/N m^{-1}	0.031	2.791	0.013	2.608
$\phi_{N,i}$/°	4.230	4.558	2.048°	1.673
k'_i/cm^{-1}/(°)^2	0.682	5.362	1.788	38.586
V_i/cm^{-1}	3400	14 900	3800	10 600

$\tilde{\nu}$—vibrational wavenumber, k_i—force constant in S_i (in linear coordinates), μ—reduced mass, $\phi_{N,i}$ –normalized angle ($v = 1$) in S_i, k'_i—force constant in S_i in angular coordinates, V_i—torsional barrier for the simultaneous flip of the two terminal rings in state S_i.

torsions of the outer phenyl rings around the two terminal bonds, as obvious from the comparison of the harmonic potential curve for the vibration τ_a with the potential of the torsion of the terminal phenyl rings around the adjacent single bonds obtained from single point (TD-)DFT calculations (Fig. 9). The barrier for the flip of one ring is calculated to $V_{0,int} = 1900\ cm^{-1}$. However, in the excited electronic state S_1, the potential curve for the torsional vibration ($\tilde{\nu}_a \approx 108\ cm^{-1}$) deviates significantly from that of the ring torsions. Due to the quinoid character of S_1, the vibrations τ_a and τ_b rather describe torsional motions of the whole molecule around the long molecular axis with one and two nodes, respectively, perpendicular to this axis. In the excited state, the barrier for the flip of one ring amounts to $5300\ cm^{-1}$.

To take into account the effect of thermal population of the excited torsional levels in S_0 on the shape of absorption and fluorescence spectra, the absorption spectrum $I(\nu)$ of the rigid molecule (*e.g.*, in solid matrices at low temperatures) is convoluted with the spectral distribution function $G_{abs}(\nu)$, which is described by an exponential

$$G_{abs}(\nu) = \exp[-\Delta(\nu)/((D-1)kT)] \quad (5)$$

where $\Delta(\nu) = P_1 - P_0$ is the energy difference, and $D = P_1/P_0$ is the energy ratio of the two vibrational potentials in S_1 and S_0. Inserting the approximations of eqn (2) or (3) into eqn (5), the difference $\Delta(\nu)$ depends on φ, while the ratio D does not. The spectral distribution function $G_{fluo}(\nu)$ of the fluorescence bands due to thermal population of excited torsional levels in S_1 is described by

$$G_{fluo}(\nu) = \exp[-\Delta(\nu)\ D/((D-1)kT)]. \quad (6)$$

Since $D > 1$, the fluorescence bands are less broadened by torsional motions than the $S_0 \rightarrow S_1$ absorption bands. Within this model we are able to simulate the absorption and fluorescence spectra of ***n*PVs** in low-viscous solvents like tetrahydrofuran (THF) quite satisfactorily (Fig. 10, top panel), after inserting values of $D = 3.8$ for **1PV**. For the longer homologues **2PV** and **3PV**, D = 5.5 and D = 7.0 are obtained, respectively.[20] In the following, the same formalism is applied to the spatially constrained situation of the PHTP channels.

The potential barriers, V_n, and the form of the torsional potential, P_n, *i.e.* its dependence on ϕ, are not available for both the dissolved state and the PHTP inclusion compound. For the band shape calculations, to the intramolecular potential, $P_{n,int}$, of the free molecules as obtained from the (TD-)DFT calculations an external potential, P_{ext}, was therefore added which accounts for impact of the solvent or for the PHTP lattice.

$$P_n = P_{n,int} + P_{ext} \quad (7)$$

The external potential is assumed to be the same in both electronic states. Thus, the spectral distribution function is modified mainly by the D-parameter, whereas Δ remains approximately constant. Upon inclusion of **2PV** into the PHTP host at room temperature, the D-parameter was reduced to $D = 1.5$, as demonstrated by comparison of the experimental absorption spectrum of **2PV** with the simulated

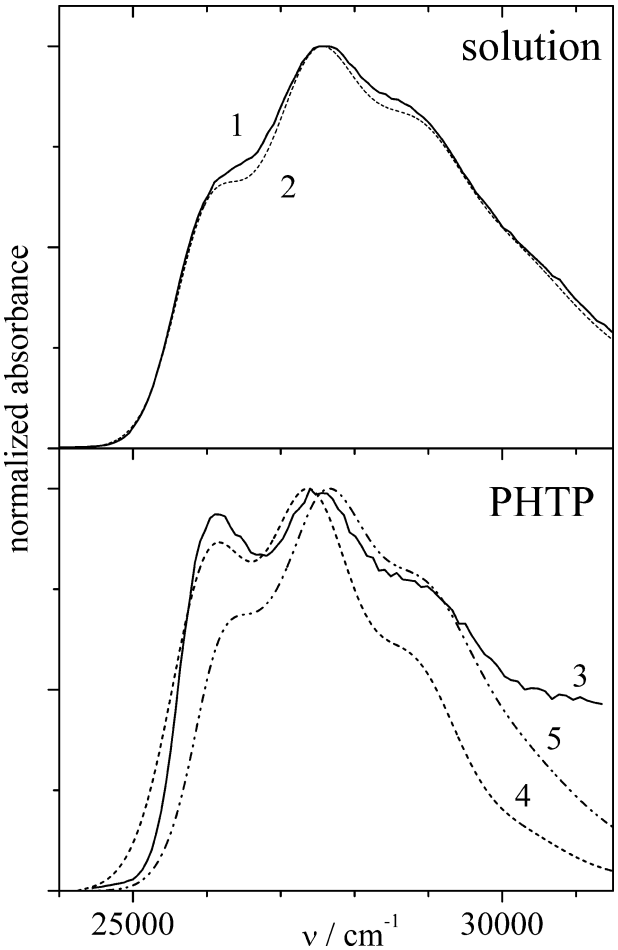

Fig. 10 Experimental (solid lines) and calculated absorption spectra of **2PV** in THF (1) and of **2PV**/**1PV**/PHTP (3). The calculated spectra are obtained by applying eqn (5) (for details see text), inserting the following D-parameters: $D = 7$ (2), $D = 1.5$ (4), $D = 5.5$ (5). The vibration sub-bands in the calculated spectra are additionally broadened with a Gaussian width of $800\ cm^{-1}$. For fitting the spectrum in PHTP, only the range between $24\,000\ cm^{-1}$ and $28\,500\ cm^{-1}$ is considered, because above $28\,500\ cm^{-1}$ the absorption of **1PV** cannot be neglected.

spectra (Fig. 10, bottom panel). This reduction in D, from $D = 5.5$ in THF to $D = 1.5$ in PHTP, supports the intuitive notion that with increasing "viscosity" of the environment, the torsional motions are more and more determined by the external potential imposed on the molecule by the surrounding "solvent".

The value of the potential barrier V_{ext} can be estimated by combining the results of the (TD-)DFT calculations and of the NMR investigations. From the (TD-)DFT single point calculation of the potential curves for the torsions of the terminal rings of **2PV** in the ground and excited electronic state of DSB *in vacuo*, a D-factor of $D \approx 4$ was deduced (Fig. 9). This value is obviously too small, mainly because the steepness of the torsional potential in the excited state is underestimated. Nevertheless it provides a reasonable starting point for the consideration of the effect of the PHTP matrix. According to the NMR measurements of the dynamics of **2PV** in PHTP, the activation energy for the ring

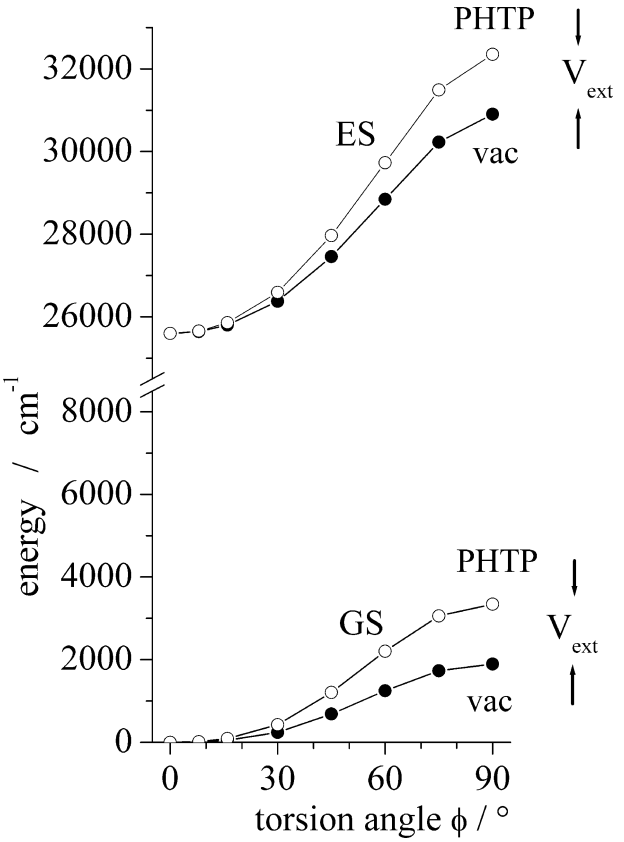

Fig. 11 Potential curves in S_0 (GS) and in S_1 (ES) for the torsion of one outer phenyl ring around C_1–C_7 in **2PV** *in vacuo* (vac) and included in PHTP (PHTP). The curves *in vacuo* are calculated on the (TD-)DFT-level (B3LYP/6-311G*). The curves for S_0 and S_1 of **2PV** in PHTP are obtained by adding the external barrier V_{ext} to the barrier *in vacuo* and linearly scaling the potential curves (for details see text).

flip of $V_0 = V_{0,int} + V_{ext} = 40$ kJ mol^{-1} = 3350 cm^{-1}, *i.e.*, the contribution of the PHTP matrix to the flip barrier amounts to $V_{0,ext} = 1450$ cm^{-1}. Adding this value to the barrier $V_{1,int}$ in S_1 yields a torsional barrier of $V_1 = 6750$ cm^{-1} (see Fig. 11). In order to obtain the potential curves P_{int} and P_{ext} for the molecule in PHTP, the intramolecular potential curves, $P_{0,int}$ and $P_{1,int}$ are then linearly scaled to render the values, V_0 and V_1, of the according rotational barriers. The value of D, resulting from the modified potential curves according to eqn (6), amounts to $D \approx 2$. Obviously, the barrier for ring flip determined by the NMR measurements is somewhat too small to fully account for the decrease to $D = 1.5$ obtained from the analysis of the UV/Vis absorption spectra.

3.3 Molecular dynamics simulations

The **2PV**/PHTP system, shown in Fig. 12, was built according to X-ray data of analogous compounds.[6] The cross sections of the pseudohexagonal nanochannels can be approximated by rectangles with dimensions of 5.9 × 8.1 Å, measured between the centers of the hydrogen atoms. Using a van der Waals radius of 1.2 Å for hydrogen, the clearance is 3.5 × 5.7 Å. The comparison of Fig. 12a and b gives an impression of the spatial constraints of **2PV** in the PHTP channels. In Fig. 12a, the guest molecule is planar, whereas in Fig. 12b the top phenyl ring is twisted by an arbitrary angle of $\phi = 15°$. In the latter conformation, the atoms of the phenyl rings and of PHTP are already in van der Waals contact. Thus, amplitudes much larger than 15° are hardly to be expected for the torsional motions of the **2PV** phenyl rings if the PHTP matrix is assumed to be rigid. This is in contradiction to the results of the NMR investigations described above, which show frequent phenyl ring flips in the **2PV**/PHTP system. In order to rationalize the results of the spectroscopic investigations, specifically the impact of the dynamics of the host channel walls on the torsional potential barrier of the guest, the intramolecular mobility of **2PV** *in vacuo* and in PHTP are investigated by molecular dynamics (MD) simulations, using the structure in Fig. 12 as starting configuration (for details see the Experimental section).

The simulations of **2PV** *in vacuo* and in PHTP at $T = 300$ K yielded the probability distributions $f(\phi)$ of the angle ϕ of the phenyl ring torsion around bond C_1–C_7 (inset of Fig. 13). *In vacuo*, a mean torsion angle of $\bar{\phi} = \frac{\int f(\phi)\phi \, d\phi}{\int f(\phi) \, d\phi} \approx 23°$ was

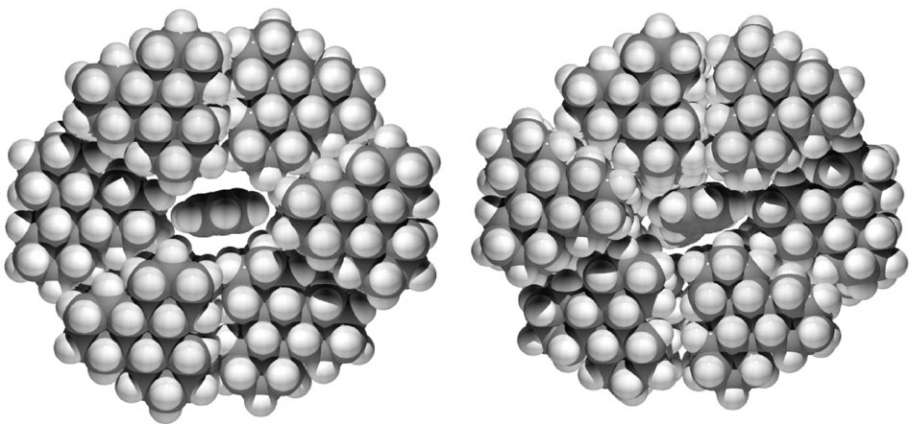

Fig. 12 Models of the system **2PV** in PHTP used for the MD simulations (view along the *c*-axis). Atomic spheres correspond to 100% of the van der Waals radii. Left: the structure as built according to X-ray data obtained on a similar system at $T = 100$ K.[6] Right: snapshot of the structure during the MD simulation at $T = 300$ K (the torsion angle of the terminal phenyl ring in **2PV** amounts to about 30°).

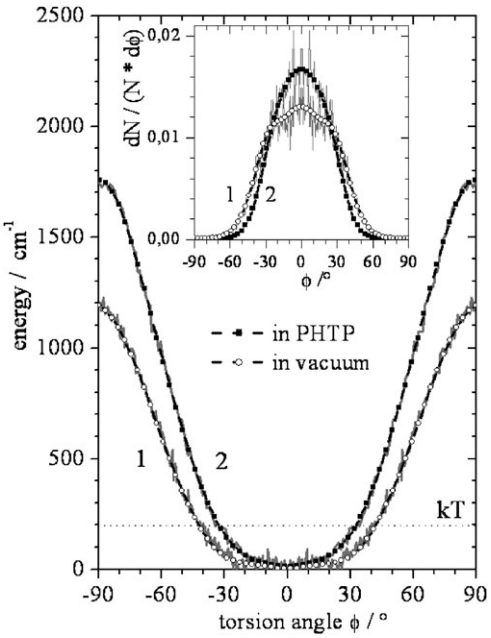

Fig. 13 Potential curves for the torsion of one of the terminal phenyl rings in **2PV** around the bond C_1–C_7 in vacuum (1) and in PHTP (2) as obtained from the probability distributions in the inset. The dashed lines are fits to these curves. The thermal energy kT at $T = 300$ K is indicated by the dotted line. Insert: Probability distributions of the torsion angles ϕ around the bond C_1–C_7 for **2PV** in vacuum (1) and included into the channels of a PHTP matrix (2) as obtained by MD simulations at $T = 300$ K (for details see text).

obtained. This value seems reasonable, considering the mean torsional amplitude of $\bar{\phi} = 30°$ obtained for **1PV** in the gas phase at 473 K,[80] from which at 293 K, assuming a harmonic potential, a value of $\bar{\phi} \approx 23°$ was estimated. Upon inclusion of **2PV** into the channels of the PHTP matrix, the mean torsion angle as obtained by the MD simulations is reduced to $\bar{\phi} \approx 18°$.

The potential curves for the ring torsion are obtained from the probability distributions using Boltzmann's law (Fig. 13). The shape of the potential curve for the ring torsion *in vacuo* is mainly determined by the superposition of the resonance energy of the conjugated π-system and of the van der Waals repulsion of the vinyl-H-atoms. At $T = 300$ K, the barrier for phenyl ring flip *in vacuo* amounts to $V_0 = 12$ cm^{-1} ($\approx$15 kJ mol^{-1}). This value is smaller than $V_0 = 1900$ cm^{-1}, as obtained from the DFT calculations, but comparable to the calculated and experimental values obtained by other groups for the ring flip in 1PV[35,77,78,81] With decreasing temperature, the MD simulations yield an increasing barrier height for the ring flip process (*e.g.* $V_0 = 1350$ cm^{-1} at $T = 100$ K). This is mainly due to the reduction of the repulsion of the vinyl H-atoms, which in turn is a consequence of the reduced amplitudes of the in-plane vinyl C–H vibrations.

According to the MD simulations, the channel walls of PHTP add an external potential of $V_{0,ext} = 550$ cm^{-1} to the potential curve for the phenyl ring torsion, which increases the ring flip barrier to $V_0 = 1750$ cm^{-1} ($\sim$22 kJ mol^{-1}). Although the MD simulations obviously underestimate the effect of the PHTP matrix on the ring flip barrier, they show that the torsional intramolecular mobility of **2PV** is significantly reduced upon inclusion into the nanochannels of PHTP. However, the channel walls are far from being rigid tubes. The role of large amplitude motions of the PHTP matrix becomes clear from an inspection of the MD simulation data where the PHTP matrix was kept rigid. In this case, the ring flip barrier assumes the unrealistically large value of $V_0 > 500$ kJ mol^{-1} which exceeds the experimental values by more than an order of magnitude.

4. Summary and conclusion

According to the results of the spectroscopic and theoretical investigations described above, the mobility of **2PV** is reduced substantially upon inclusion into the channels of PHTP. Nevertheless, there is significant mobility left. NMR spectroscopy shows an overall, wobble-like motion which above $T = 320$ K is superimposed by local ring flips. At room temperature, fluorescence spectroscopy reveals residual intramolecular torsional mobility which is removed only upon cooling of the samples to $T = 10$ K, where also intermolecular vibrations are frozen in. Temperature dependent NMR measurements, together with fluorescence spectroscopic investigations and MD studies thus provide a consistent picture of the degree of immobilization of the guest molecule.

The overall wobble process of the guest molecules displays a strong temperature dependence which can be attributed to the strong sterical hindrance imposed by the PHTP host lattice. The activation energy of $E_A = 40$ kJ mol^{-1} for the ring flip motion, derived from variable temperature NMR studies, is almost twice that calculated for the rotation of the central ring in vacuum[82] and three times that calculated for the flip of a single ring in stilbene ($E_A \approx 13$ kJ mol^{-1}).[35,79] This confirms the results obtained by earlier investigations[32,44] that in channels of pseudohexagonal symmetry, molecular motions, such as the present ring flips, are strongly hindered by the walls of the PHTP channels, as also suggested by the results of our MD simulations. It should be mentioned that kinetic parameters exist for the reorientational motions of a series of small molecules, such as benzene, trioxane, cyclohexane, *etc.* in thiourea, urea or cyclophosphazene inclusion compounds.[21,38,39,41,43] For these systems much smaller values for the activation parameters of the overall reorientational motions were reported. Moreover, the overall motions of those guest species were found to occur on a much faster timescale and therefore reach the NMR "fast motional" limit in some cases even far below 100 K. Both findings can be understood by the fact that in those studies much smaller guest species were involved whose overall mobility is spatially (and thus also thermally) less hindered than in the present case.

After combining the evidence of our spectroscopic and theoretical investigations, the following picture for the motion of **2PV** in PHTP emerges. The internal stretch and deformation vibrations of guest and host molecules lead to a diffusive reorientation of **2PV** inside the channel, which is seen by ^{2}H NMR spectroscopy as a wobble-in-cone motion. The respective pre-exponential factor of $A = 5.1 \times 10^{13}$ s^{-1} is close to the frequencies of the C–C and C–H vibrations driving this

process. At the same time, the intramolecular torsional motions of **2PV** lead to a blurring of the fluorescence excitation spectra. At $T > 320$ K these torsional vibrations lead to a measurable rate of ring flips, similar to what has been previously observed in stretched sheets of deuterated PPV.[22] Again, for this intramolecular type of motion, the pre-exponential factor of $A = 1.4 \times 10^{12}\ s^{-1}$ shows reasonable agreement with the calculated frequencies of the torsional vibrations ($\nu_0 \approx 9 \times 10^{11}\ s^{-1}$). The observed activation energies of around 40 kJ mol^{-1} for both processes are larger than, but still comparable to the results of MD simulations of **2PV** included into the channels of a non-rigid PHTP matrix. When the PHTP matrix is kept rigid during the simulation runs, unrealistically high activation barriers of >500 kJ mol^{-1} for the ring flips are obtained. This confirms the results of earlier investigations on PHTP[44,45] and on zeolite[83] systems which clearly demonstrate that the dynamics of the matrix plays an important role for the mobility of the included guest molecules.

Acknowledgements

This work was supported by the European Commission through the Human Potential Program (RTN "Nanochannel" Contract No. HPRN-CT-2002-00323 and RTN "Nanomatch Contract No. MRTN-CT-2006-035884) and by the Deutsche Forschungsgemeinschaft (Graduiertenkolleg "Chemie in Interphasen", Grant No. 441/2, and "Moderne Methoden der magnetischen Resonanz in der Materialforschung", Grant No. 448). R.M.-A. thanks the Alexander von Humboldt Foundation (Germany) for a grant. B.M.M. thanks the Ministerio de Ciencia e innovacion (MICINN) of Spain for a postdoctoral grant and a 'Juan de la Cierva' contract. J.G. is 'Ramón y Cajal' research fellow, financed by the MICINN. At present he is a visiting researcher at the ICMol, Valencia, through the Consolider Ingenio 2010 "Molecular Nanoscience" activity of the MICINN. The work in Mons is partly supported by the EU through the Marie Curie Research Training Network THREADMILL (MRTN-CT-2006-036040) and by the Belgian National Science Foundation (FNRS/FRFC). J. C. is a senior research associate and D.B. research director of FNRS.

References

1 D. Oelkrug, H.-J. Egelhaaf, D. Worrall and F. Wilkinson, *J. Fluoresc.*, 1995, **5**, 165.
2 D. Oelkrug, A. Tompert, J. Gierschner, H.-J. Egelhaaf, M. Hanack, M. Hohloch and E. Steinhuber, *J. Phys. Chem. B*, 1998, **102**, 1902.
3 R. Pacios, A. Chatten, K. J. Kawano, J. R. Durrant, D. D. C. Bradley and J. Nelson, *Adv. Funct. Mater.*, 2006, **16**, 2117.
4 L. Lüer, H.-J. Egelhaaf, D. Oelkrug, G. Cerullo, G. Lanzani, B.-H. Huisman and D. deLeeuw, *Org. Electron.*, 2004, **5**, 83.
5 K. K. Lin, S.-J. Chua and W. Wang, *Thin Solid Films*, 2002, **417**, 36.
6 O. König, H.-B. Bürgi, T. Armbruster, J. Hulliger and T. Weber, *J. Am. Chem. Soc.*, 1997, **119**, 10632.
7 C. Botta, R. Ferro, G. Di Silvestro and R. Tubino, *Supramolecular Photosensitive and Electroactive Materials*, ed. H. S. Nalwa, Academic Press, San Diego/CA, USA, 1st edn, 2001, pp. 439–524.
8 J. Gierschner, L. Lüer, D. Oelkrug, E. Musluoglu, B. Behnisch and M. Hanack, *Adv. Mater.*, 2000, **12**, 757.
9 J. Gierschner, L. Lüer, D. Oelkrug, E. Musluoglu, B. Behnisch and M. Hanack, *Synth. Met.*, 2001, **121**, 1695.
10 J. Gierschner, H.-J. Egelhaaf, H.-G. Mack, D. Oelkrug, R. M. Alvarez and M. Hanack, *Synth. Met.*, 2003, **137**, 1449.
11 G. Bongiovanni, C. Botta, J. E. Communal, F. Cordella, L. Magistrelli, A. Mura, G. Patrinoiu, P. Picouet and G. DiSilvestro, *Mater. Sci. Eng., C*, 2003, **23**, 909.
12 C. Botta, S. Destri, M. Pasini, P. Picouet, G. Bongiovanni, A. Mura, M. Uslenghi, G. Di Silvestro and R. Tubino, *Synth. Met.*, 2003, **139**, 791.
13 C. Botta, G. Bongiovanni, A. Mura, G. Di Silvestro and R. Tubino, *Synth. Met.*, 2001, **116**, 175.
14 M. A. Loi, A. Mura, G. Bongiovanni, C. Botta, G. Di Silvestro and R. Tubino, *Synth. Met.*, 2001, **121**, 1299.
15 G. Bongiovanni, C. Botta, G. Di Silvestro, M. A. Loi, A. Mura and R. Tubino, *Chem. Phys. Lett.*, 2001, **345**, 386.
16 C. Botta, R. Treviganti, G. Bongiovanni, A. Mura and R. Tubino, *Synth. Met.*, 1999, **101**, 565.
17 M. Farina, G. Di Silvestro and P. Sozzani, *Comp. Supramol. Chem.*, 1996, **6**, 371.
18 L. Poulsen, M. Jazdzyk, J.-E. Communal, J. C. Sancho-García, A. Mura, G. Bongiovanni, D. Beljonne, J. Cornil, M. Hanack, H.-J. Egelhaaf and J. Gierschner, *J. Am. Chem. Soc.*, 2007, **129**, 8585.
19 J. C. Sancho-García, L. Poulsen, J. Gierschner, R. Martínez-Alvárez, E. Hennebicq, M. Hanack, H.-J. Egelhaaf, D. Oelkrug, D. Beljonne, J. L. Brédas and J. Cornil, *Adv. Mater.*, 2004, **16**, 1193.
20 J. Gierschner, H.-G. Mack, L. Lüer and D. Oelkrug, *J. Chem. Phys.*, 2002, **116**, 8596.
21 A. Liebelt, A. Detken and K. Müller, *J. Phys. Chem. B*, 2002, **106**, 7781.
22 J. H. Simpson, D. M. Rice and F. E. Karasz, *Macromolecules*, 1992, **25**, 2099.
23 P. Sozzani, A. Comotti, S. Bracco and R. Simonutti, *Chem. Commun.*, 2004, 768.
24 P. Sozzani, R. Simonutti, S. Bracco and A. Comotti, *Polym. Prepr.*, 2003, **44**, 297.
25 R. Simonutti, M. Mauri, S. Bracco, A. Comotti and P. Sozzani, *Polym. Prepr.*, 2003, **44**, 361.
26 F. C. Schilling, K. R. Amundson and P. Sozzani, *Macromolecules*, 1994, **27**, 6498.
27 P. Sozzani, F. A. Bovey and F. C. Schilling, *Macromolecules*, 1991, **24**, 6764.
28 F. C. Schilling, P. Sozzani and F. A. Bovey, *Macromolecules*, 1991, **24**, 4369.
29 F. C. Schilling, F. A. Bovey and P. Sozzani, *Polym. Prepr.*, 1990, **31**, 113.
30 G. Di Silvestro, P. Sozzani and M. Farina, *Mol. Cryst. Liq. Cryst.*, 1990, **187**, 383.
31 P. Sozzani, R. W. Behling, F. C. Schilling, S. Bruckner, E. Helfand, F. A. Bovey and L. W. Jelinski, *Macromolecules*, 1989, **22**, 3318.
32 P. Sozzani, F. A. Bovey and F. C. Schilling, *Macromolecules*, 1989, **22**, 4225.
33 S. Bruckner, P. Sozzani, C. Boeffel, S. Destri and G. Di Silvestro, *Macromolecules*, 1989, **22**, 607.
34 M. Brustolon, A. Barbon, M. Bortolus, A. L. Maniero, P. Sozzani, A. Comotti and R. Simonutti, *J. Am. Chem. Soc.*, 2004, **126**, 15512.
35 E. Meirovitch, I. Belsky and S. Vega, *J. Phys. Chem.*, 1984, **88**, 1522.
36 A. E. Aliev and K. D. M. Harris, *J. Phys. Chem. A*, 1997, **101**, 4541.
37 J. A. Villanueva-Garibay and K. Müller, *Lect. Notes Phys.*, 2006, **684**, 65.
38 J. A. Villanueva-Garibay and K. Müller, *J. Phys. Chem. B*, 2004, **108**, 15057.
39 R. Poupko, E. Furman, K. Müller and Z. Luz, *J. Phys. Chem.*, 1991, **95**, 405.
40 E. Gelerinter, Z. Luz, R. Poupko and H. Zimmermann, *J. Phys. Chem.*, 1990, **94**, 5391.
41 K. Müller, *J. Phys. Chem.*, 1992, **96**, 5733.
42 K. Müller, *Magn. Reson. Chem.*, 1995, **33**, 113.
43 J. Schmider and K. Müller, *J. Phys. Chem. A*, 1998, **102**, 1181.
44 R. Dodge and W. L. Mattice, *Macromolecules*, 1991, **24**, 2709.
45 T. Haliloglu and W. L. Mattice, *Macromol. Symp.*, 1996, **101**, 435.

46 Y. Zhan and W. L. Mattice, *Macromolecules*, 1992, **25**, 3439.
47 Y. Zhan and W. L. Mattice, *Macromolecules*, 1992, **25**, 4078.
48 R. Tubino, E. Fois, A. Gamba, G. Macchi, F. Meinardi and A. Minoia, in *Studies in Surface Science and Catalysis*, ed. A. Gamba, C. Collela and S. Collucia, Elsevier, Amsterdam, The Netherlands, 2005, vol. 155, p. 501.
49 S. O. Vásquez, *Comput. Mater. Sci.*, 2006, **37**, 572.
50 Z. Yang, F. E. Karasz and J. Geise, *Macromolecules*, 1993, **26**, 6570.
51 J. Hulliger, O. König and R. Hoss, *Adv. Mater.*, 1995, **7**, 719.
52 A. D. Becke, *J. Chem. Phys.*, 1993, **98**, 1372.
53 For the TURBOMOLE calculations basis sets were obtained from the Extensible Computational Chemistry Environment Basis Set Database, Version 02/25/04, as developed and distributed by the Molecular Science Computing Facility, Environmental and Molecular Sciences Laboratory which is part of the Pacific Northwest Laboratory, P.O. Box 999, Richland, Washington 99352, USA, and funded by the U.S. Department of Energy. The Pacific Northwest Laboratory is a multi-program laboratory operated by Battelle Memorial Institute for the U.S. Department of Energy under contract DE-AC06-76RLO 1830. Contact Karen Schuchardt for further information.
54 R. Ahlrichs, *et al.*, *TURBOMOLE, version 5.71*, Universität Karlsruhe, Karlsruhe, 2003.
55 J. W. Ponder, *TINKER: Software Tools for Molecular Design, 4.2*, Washington University School of Medicine, Saint Louis, MO, 2004.
56 (*a*) S. Kumar, D. Bouzida, R. H. Swendsen, P. A. Kollman and J. M. Rosenberg, *J. Comput. Chem.*, 1992, **13**, 1011; (*b*) WHAM code: http://membrane.urmc.rochester.edu/.
57 S. Lefrant, J. P. Buisson, M. Baitoul and I. Orion, *Pure Appl. Opt.*, 1996, **5**, 613.
58 J. H. Simpson, N. Egger, M. A. Masse, D. M. Rice and F. E. Karasz, *J. Polym. Sci., Part B: Polym. Phys.*, 1990, **28**, 1859.
59 E. R. deAzebedo, R. W. A. Franco, A. Marletta, R. M. Faria and T. Bonagamba, *J. Chem. Phys.*, 2003, **119**, 2923.
60 P. Sozzani, R. Simonutti and A. Comotti, *Mol. Cryst. Liq. Cryst.*, 1996, **227**, 299.
61 M. M. Maricq and J. S. Waugh, *J. Chem. Phys.*, 1979, **70**, 3300.
62 D. Suwelack, W. P. Rothwell and J. S. Waugh, *J. Chem. Phys.*, 1980, **73**, 2559.
63 A. D. Ronemus, R. R. Vold and R. L. Vold, *J. Chem. Soc., Faraday Trans. 1*, 1988, **84**, 3761.
64 O. Yano and Y. Wada, *J. Polym. Sci., Part A2*, 1971, **9**, 669.
65 A. V. Lyulin, N. K. Balabaev and M. A. J. Michels, *Macromolecules*, 2002, **35**, 9595.
66 T. Bräuniger, R. Poupko and Z. Luz, *J. Chem. Phys.*, 2000, **112**, 10858.
67 P. Speier, A. Müller, C. Meinel and U. Haeberlen, *Mol. Phys.*, 1998, **95**, 859.
68 G. A. Facey, T. J. Connolly, C. Bensimon and T. Durst, *Can. J. Chem.*, 1996, **74**, 1844.
69 T. Hiraoki, A. Kogame, N. Nishi and A. Tsutsumi, *J. Mol. Struct. (THEOCHEM)*, 1998, **441**, 243.
70 M. A. Keniry, T. M. Rothgeb, R. L. Smith, H. S. Gutowsky and E. Oldfield, *Biochemistry*, 1983, **22**, 1917.
71 M. A. Kennedy, R. R. Vold and R. L. Vold, *J. Magn. Reson.*, 1991, **91**, 301.
72 M. H. Wann and G. S. Harbison, *J. Chem. Phys.*, 1994, **101**, 231.
73 J. H. Simpson, D. M. Rice and F. M. Karasz, *J. Polym. Sci., Part B: Polym. Phys.*, 1992, **30**, 11.
74 H.-J. Egelhaaf, L. Lüer, A. Tompert, P. Bäuerle, K. Müllen and D. Oelkrug, *Synth. Met.*, 2000, **115**, 63.
75 F.-C. Hsu, M. Hayashi, H.-W. Wang, S. H. Lin and J.-K. Wang, *J. Phys. Chem. A*, 2007, **111**, 759.
76 T. Suzuki, N. Mikami and M. Ito, *J. Phys. Chem.*, 1986, **90**, 6431.
77 J. Laane, *J. Phys. Chem. A*, 2000, **104**, 7715.
78 S. P. Kwasniewski, L. Claes and J. P. Francois, *J. Chem. Phys.*, 2003, **118**, 7823.
79 O. Lhost and J. L. Bredas, *J. Chem. Phys.*, 1992, **96**, 5279.
80 M. Trætteberg, E. B. Frantsen, F. C. Mijehoff and A. Hoeckstra, *J. Mol. Struct. (THEOCHEM)*, 1975, **26**, 57.
81 S. P. Kwasniewski, J. P. Francois and M. S. Deleuze, *J. Phys. Chem. A*, 2003, **107**, 5168.
82 G. C. Claudio and E. R. Bittner, *Chem. Phys.*, 2002, **276**, 81.
83 P. C. M. M. Magusin and R. A. van Santen, *Chem. Phys. Lett.*, 2003, **373**, 630.